RACE 2 SPACE

Kimchi

Propulsion Systems(?)

Race 2 Space 2026 Submission

Kimchi Engine

Critical Design Review

Regeneratively Cooled LOX/Ethanol Lander Engine

Project:	Kimchi Engine Program
Document:	Critical Design Review (CDR)
Team:	Kimchi Team
Date:	April 2026
Configuration:	IN718 1300N Lander Engine

Contents

1 System Overview

1.1 Engine System Definition

1.1.1 Design Details

The Kimchi engine is a pressure-fed, throttleable LOX/ethanol rocket engine configured as a finalized hot-fire configuration for the Race 2 Space campaign. The flight-like hot-gas path consists of an impinging injector, an Inconel 718 chamber and conical nozzle, and a fuel-side regenerative cooling circuit that routes ethanol from the nozzle exit region to the injector. The design point is 1300 N thrust at 15.0 bar chamber pressure with fixed geometry retained through the full throttle band. The operating throttle ratio is $R = 0.40$ to 1.00.

1.1.2 Method / Model Used

Performance sizing is closed from frozen-at-throat NASA CEA results with a characteristic-velocity efficiency derate. The governing system relations are

$$c^*_{\text{eff}} = \eta_{c^*} c^*_{\text{ideal}}, \tag{1}$$

$$\dot{m} = \frac{F}{C_f c^*_{\text{eff}}}, \tag{2}$$

$$A_t = \frac{\dot{m} c^*_{\text{eff}}}{P_c}, \tag{3}$$

$$\epsilon = \frac{A_e}{A_t}. \tag{4}$$

Here $\eta_{c^*} = 0.89$, F is thrust, C_f is thrust coefficient, $\dot{m}$ is total mass flow, A_t is throat area, and A_e is exit area.

1.1.3 Numerical Results

At the design point, $F = 1300\,\text{N}$, $C_f = 1.3247$, and $c^*_{\text{eff}} = 1401.9\,\text{m/s}$. Equation (2) gives $\dot{m} = 0.700\,\text{kg/s}$. With $P_c = 15.0\,\text{bar} = 1.50 \times 10^6\,\text{Pa}$, Equation (3) gives $A_t = 6.54 \times 10^{-4}\,\text{m}^2$, corresponding to a 28.86 mm throat diameter. Table 1 lists the finalized system values, and Figure 1 shows the assembly definition.

1.1.4 Assessment

The design point in Table 1 is analytically self-consistent with the fixed geometry, the pressure-fed supply limits, the regenerative thermal solution, and the structural screening summarized later in this document. These values define the baseline prediction set that will later be compared against assembly checkout and hot-fire data. The same finalized geometry is used for the throttle, thermal, and structural sweeps; no subsystem is re-optimized off-design.

Table 1: Final engine definition

Parameter	Final value
Propellants	Liquid oxygen / ethanol
Design thrust	1300 N
Throttle range	40 % to 100 %
Chamber-pressure range	6.0 bar to 15.0 bar
Mixture ratio	$O/F = 1.0$
Total mass-flow range	0.280 kg/s to 0.700 kg/s
Analysis-ambient specific impulse range	160.5 s to 189.4 s
Design-point vacuum specific impulse	208.6 s
Chamber material	Inconel 718
Cooling method	Fuel regenerative cooling, exit-to-injector flow
Gas-side model	NASA CEA, frozen at throat, Bartz convection with 20% knockdown
Coolant-side model	Gnielinski convection with Naraghi fin-efficiency correction
Structural model	Chamber thin-wall membrane plus thermal-gradient stress with buckling screen; separate thrust-structure FEA screening

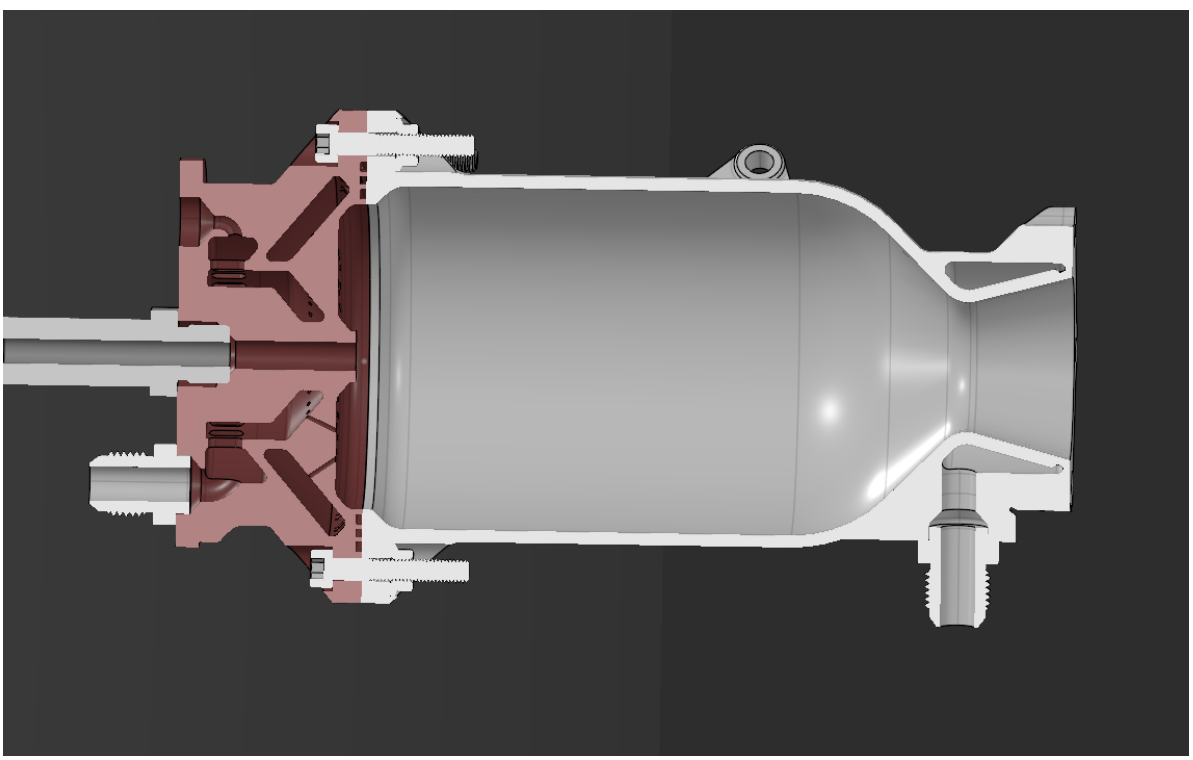

Figure 1: Final engine assembly used as the system definition for this CDR.

To give the reader a faster visual map of the hardware, Figure 2 reproduces the annotated engine-overview slide used in the presentation deck.

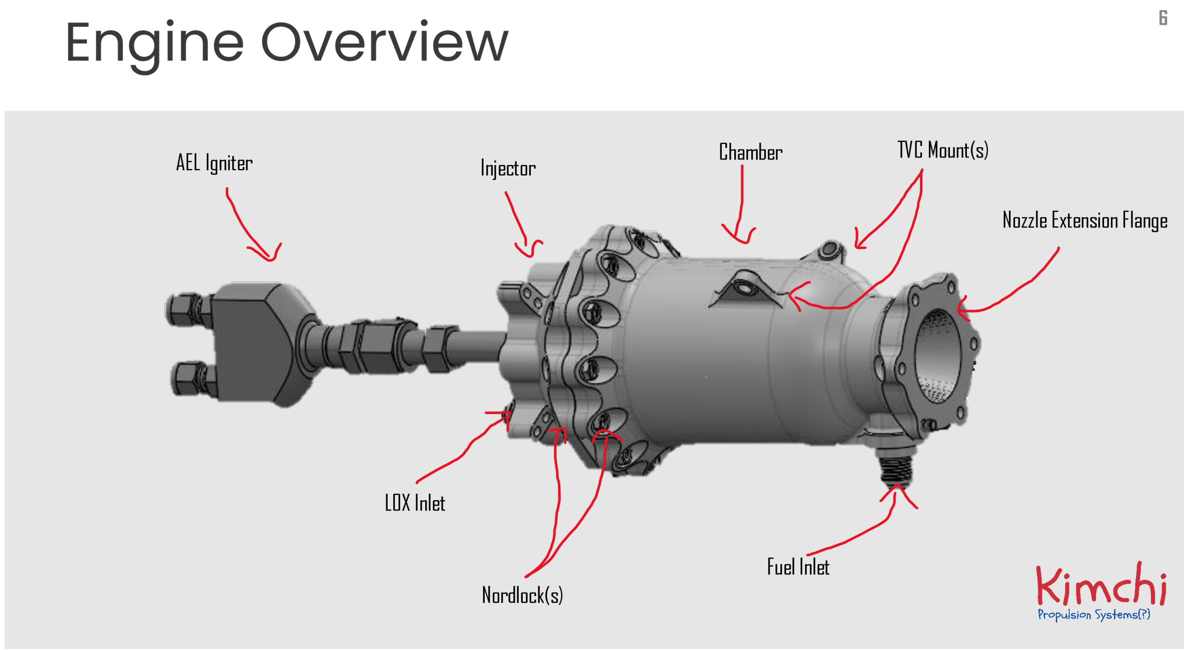

Figure 2: Annotated engine-overview slide from the presentation deck showing the igniter, injector, chamber, mounts, and propellant interfaces.

1.2 Performance Envelope

1.2.1 Design Details

The finalized hardware is throttled by reducing chamber pressure while holding chamber, throat, exit, and injector geometry fixed. The performance envelope therefore represents the fabricated article rather than a resized family of engines.

1.2.2 Method / Model Used

The throttle sweep is governed by

$$P_c(R) = RP_{c,0}, \tag{5}$$

$$\dot{m}(R) = \frac{P_c(R)A_t}{c^*_{\text{eff}}(R)}, \tag{6}$$

$$F(R) = \dot{m}(R)C_f(R)c^*_{\text{eff}}(R). \tag{7}$$

The design chamber pressure reference is $P_{c,0} = 15.0\,\text{bar}$, and R is the commanded throttle ratio.

Table 2: Throttle sweep endpoint summary

Point	P_c	Thrust	$\dot{m}$	I_{sp}	C_f	P_e	Analytical note
$R = 0.40$	6.000 bar	440.6 N	0.280 kg/s	160.5 s	1.1225	0.680 bar	Stable low-throttle operating point
$R = 1.00$	15.000 bar	1300.0 N	0.700 kg/s	189.4 s	1.3247	1.700 bar	Design-point requirement satisfied

1.2.3 Numerical Results

1.2.4 Assessment

Table 2 and Figure 3 show the predicted fixed-geometry sweep results. The design-point thrust relation is recovered directly from Equation (7): $0.700\,\text{kg/s} \times 1.3247 \times 1401.9\,\text{m/s} = 1300.0\,\text{N}$. Within the current model, the minimum-throttle point remains above 440 N with the same hardware, indicating a continuous 40 % to 100 % operating band without geometry changes. Hot-fire thrust and chamber-pressure data will be compared against these predicted points.

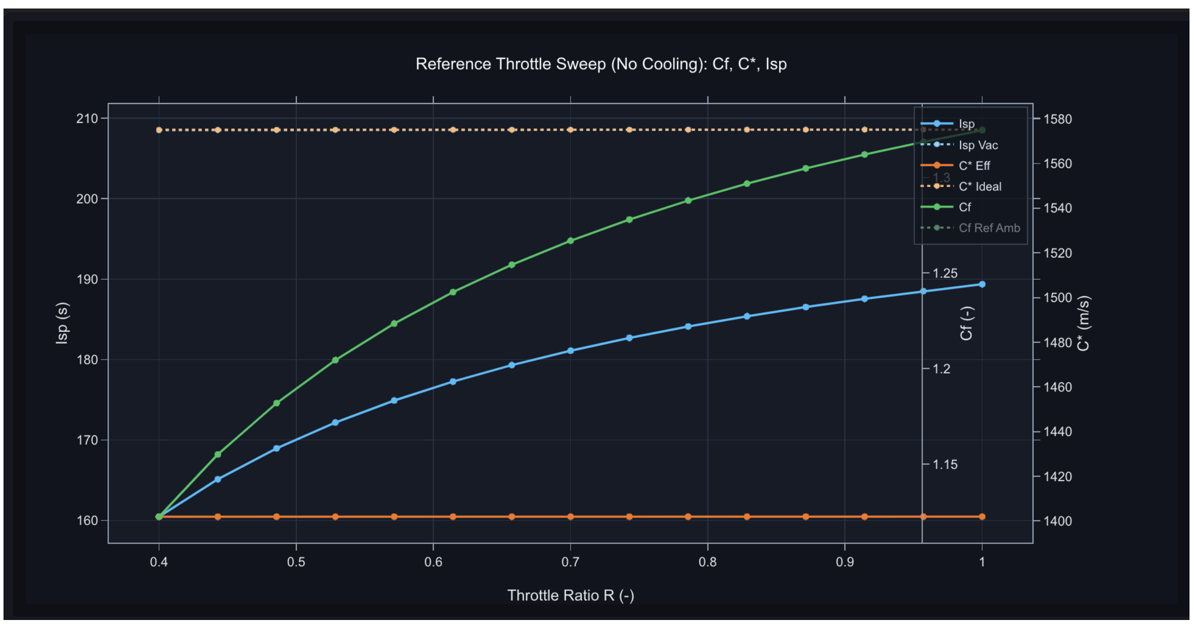

Figure 3: Fixed-geometry throttle sweep showing thrust, mass flow, and specific impulse across the finalized operating range.

Figure 4 reproduces the full 15-point throttle table from the presentation deck so the closed chamber-pressure, performance, and feed-pressure states can be read directly in the report.

Figure 5 adds the companion presentation-deck performance plot showing the sweep-wise variation in C_f, delivered c^*, and specific impulse.

Throttle Per-Level Specifications

19

#	Throttle	O/F	Pc	Thrust	mdot	Cf	C* Eff	C* Ideal	Isp	Isp Vac	Tc	Pe	Ox dP/Pc	Fuel dP/Pc	Ox Supply P	Fuel Supply P	Ox Injector-End P	Fuel Injector-End P
1	R=0.40	1.000	6.000 bar	440.6 N	0.2800 kg/s	1.1225	1401.9 m/s	1575.2 m/s	160.5 s	208.5 s	2345.3 K	0.680 bar	0.300	0.300	7.800 bar	7.800 bar	7.800 bar	7.800 bar
2	R=0.44	1.000	6.643 bar	502.0 N	0.3100 kg/s	1.1551	1401.9 m/s	1575.2 m/s	165.1 s	208.5 s	2346.1 K	0.752 bar	0.332	0.332	8.849 bar	8.849 bar	8.849 bar	8.849 bar
3	R=0.49	1.000	7.286 bar	563.4 N	0.3400 kg/s	1.1820	1401.9 m/s	1575.2 m/s	169.0 s	208.5 s	2346.8 K	0.825 bar	0.364	0.364	9.940 bar	9.940 bar	9.940 bar	9.940 bar
4	R=0.53	1.000	7.929 bar	624.8 N	0.3700 kg/s	1.2045	1401.9 m/s	1575.2 m/s	172.2 s	208.5 s	2347.4 K	0.898 bar	0.396	0.396	11.072 bar	11.072 bar	11.072 bar	11.072 bar
5	R=0.57	1.000	8.571 bar	686.1 N	0.4000 kg/s	1.2236	1401.9 m/s	1575.2 m/s	174.9 s	208.6 s	2348.0 K	0.971 bar	0.429	0.429	12.245 bar	12.245 bar	12.245 bar	12.245 bar
6	R=0.61	1.000	9.214 bar	747.5 N	0.4300 kg/s	1.2400	1401.9 m/s	1575.2 m/s	177.3 s	208.6 s	2348.5 K	1.044 bar	0.461	0.461	13.459 bar	13.459 bar	13.459 bar	13.459 bar
7	R=0.66	1.000	9.857 bar	808.9 N	0.4600 kg/s	1.2544	1401.9 m/s	1575.2 m/s	179.3 s	208.6 s	2348.9 K	1.117 bar	0.493	0.493	14.715 bar	14.715 bar	14.715 bar	14.715 bar
8	R=0.70	1.000	10.500 bar	870.3 N	0.4900 kg/s	1.2669	1401.9 m/s	1575.2 m/s	181.1 s	208.6 s	2349.3 K	1.190 bar	0.525	0.525	16.012 bar	16.012 bar	16.012 bar	16.012 bar
9	R=0.74	1.000	11.143 bar	931.7 N	0.5200 kg/s	1.2780	1401.9 m/s	1575.2 m/s	182.7 s	208.6 s	2349.7 K	1.263 bar	0.557	0.557	17.351 bar	17.351 bar	17.351 bar	17.351 bar
10	R=0.79	1.000	11.786 bar	993.1 N	0.5500 kg/s	1.2879	1401.9 m/s	1575.2 m/s	184.1 s	208.6 s	2350.0 K	1.336 bar	0.589	0.589	18.731 bar	18.731 bar	18.731 bar	18.731 bar
11	R=0.83	1.000	12.429 bar	1.054 kN	0.5800 kg/s	1.2968	1401.9 m/s	1575.2 m/s	185.4 s	208.6 s	2350.3 K	1.408 bar	0.621	0.621	20.152 bar	20.152 bar	20.152 bar	20.152 bar
12	R=0.87	1.000	13.071 bar	1.116 kN	0.6100 kg/s	1.3048	1401.9 m/s	1575.2 m/s	186.5 s	208.6 s	2350.6 K	1.481 bar	0.654	0.654	21.614 bar	21.614 bar	21.614 bar	21.614 bar
13	R=0.91	1.000	13.714 bar	1.177 kN	0.6400 kg/s	1.3121	1401.9 m/s	1575.2 m/s	187.6 s	208.6 s	2350.9 K	1.554 bar	0.686	0.686	23.118 bar	23.118 bar	23.118 bar	23.118 bar
14	R=0.96	1.000	14.357 bar	1.239 kN	0.6700 kg/s	1.3187	1401.9 m/s	1575.2 m/s	188.5 s	208.6 s	2351.2 K	1.627 bar	0.718	0.718	24.663 bar	24.663 bar	24.663 bar	24.663 bar
15	R=1.00	1.000	15.000 bar	1.300 kN	0.7000 kg/s	1.3247	1401.9 m/s	1575.2 m/s	189.4 s	208.6 s	2351.4 K	1.700 bar	0.750	0.750	26.249 bar	26.249 bar	26.249 bar	26.249 bar

Kimchi
Propulsion Systems(?)

Figure 4: Per-level throttle specification table from the presentation deck listing the full fixed-geometry sweep, delivered performance, and injector-end/supply-pressure states.

Throttle Per-Level Performance

25

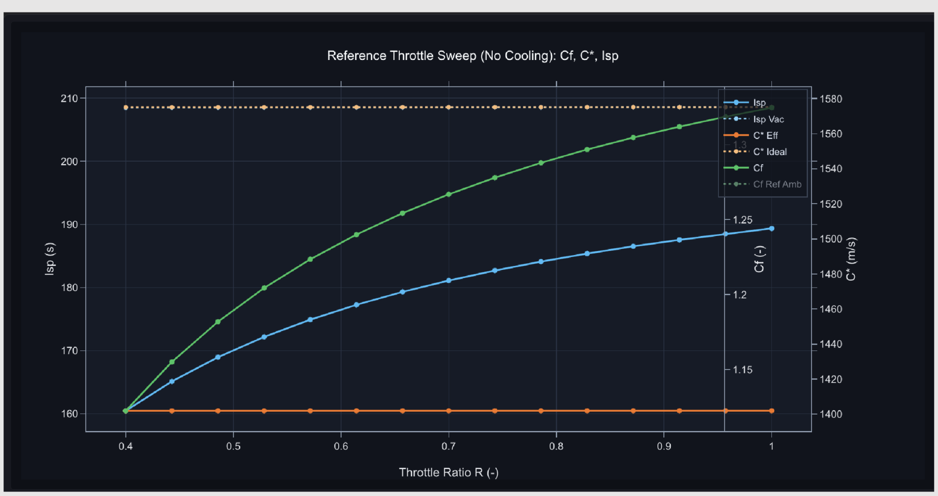

Kimchi
Propulsion Systems(?)

Figure 5: Per-level performance plot from the presentation deck showing C_f, delivered c^*, and specific impulse across the fixed-geometry throttle schedule.

2 Injector Subsystem

2.1 Injector Body and Metering

2.1.1 Design Details

The injector subsystem uses a center-fed impinging architecture integrated with propellant manifolds, seal grooves, bolt-circle retention, and dedicated pressure and temperature pickup locations. LOX is delivered directly to the injector. Ethanol is routed through the regenerative cooling circuit and enters the injector after the fuel-side thermal-hydraulic path. The injector hardware is therefore the hydraulic closure point for both feed circuits. Figure 6 shows the injector face geometry, and Figure 7 shows the manifold and passage layout used for this release.

Figure 8 complements the CAD cutaway with the annotated injector slide used in the presentation material, highlighting the inlet and sensor features at the injector body.

2.1.2 Method / Model Used

The injector is sized once at minimum throttle and then held at fixed effective hydraulic area through the full sweep. The governing metering relations are

$$\dot{m} = C_d A \sqrt{2\rho \Delta P_{\text{inj}}}, \tag{8}$$

$$\Delta P_{\text{inj}} = \frac{1}{2\rho}\left(\frac{\dot{m}}{C_d A}\right)^2, \tag{9}$$

$$P_{\text{inj,end}} = P_c + \Delta P_{\text{inj}}, \tag{10}$$

$$P_{\text{fuel,supply}} = P_{\text{inj,end}} + \Delta P_{\text{regen}}. \tag{11}$$

The minimum-throttle injector design rule is $\Delta P_{\text{inj}}/P_c = 0.30$ on both propellant sides.

2.1.3 Numerical Results

Table 3: Injector and feed-system closure

Point	ΔP_{inj}	$P_{\text{inj,end}}$	ΔP_{regen}	LOX supply pressure	Fuel supply pressure	Margin to 28 bar cap
$R = 0.40$	1.800 bar	7.800 bar	0.071 bar	7.800 bar	7.871 bar	20.129 bar fuel-side minimum
$R = 1.00$	11.249 bar	26.249 bar	0.498 bar	26.249 bar	26.748 bar	1.252 bar fuel-side minimum

2.1.4 Assessment

Table 3 and Figure 9 summarize the predicted injector pressure closure. At minimum throttle, the finalized injector relation is explicit: $\Delta P_{\text{inj}} = 0.30 \times 6.0\,\text{bar} = 1.8\,\text{bar}$, so Equation (10) gives

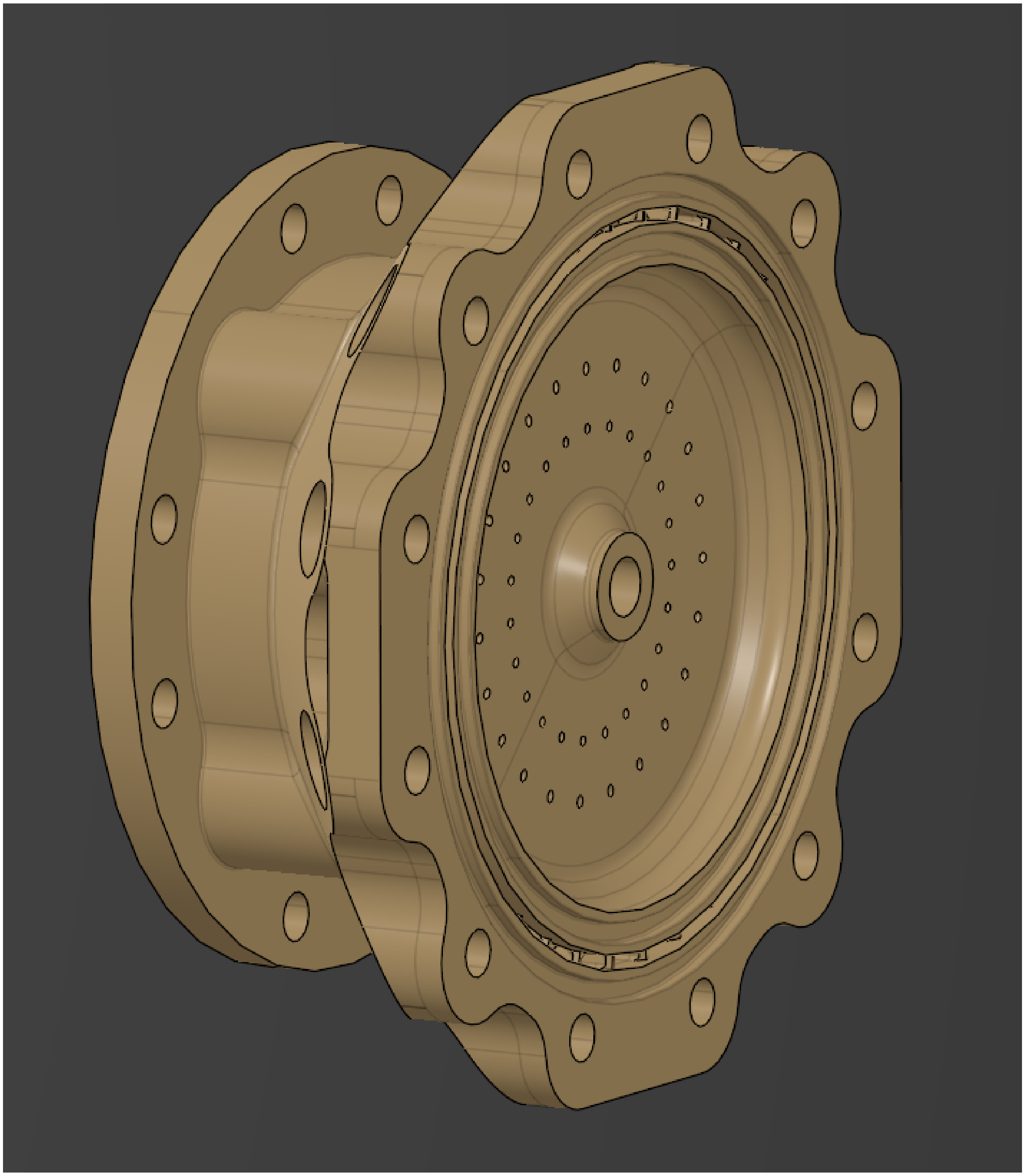

Figure 6: Injector face geometry and bolt pattern retained for the final hardware configuration.

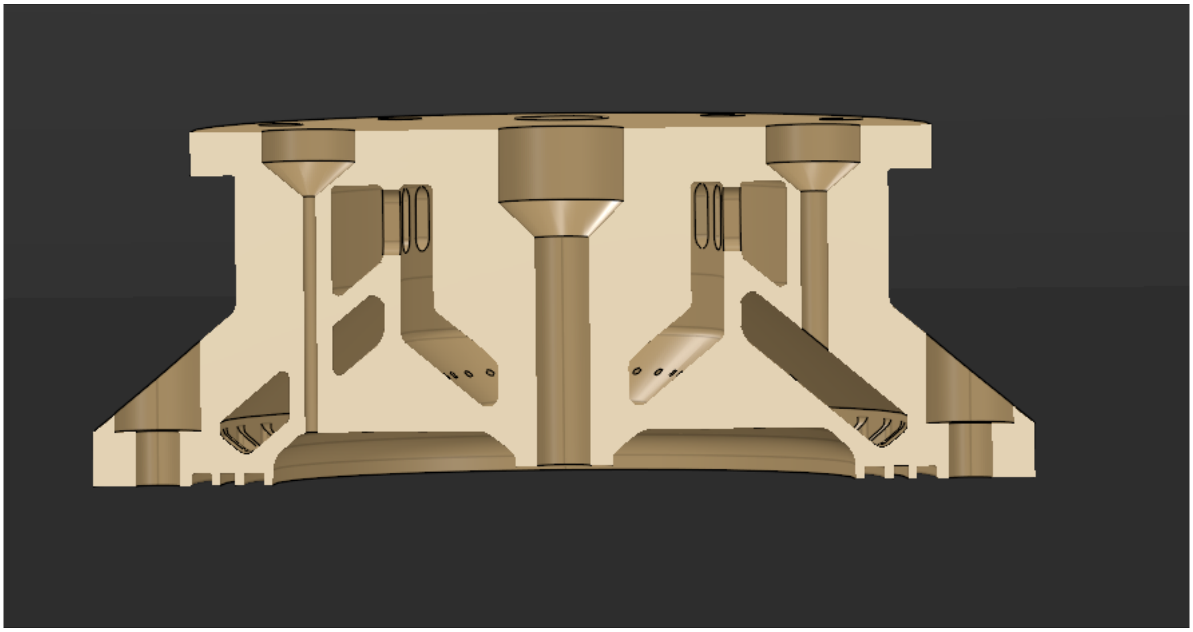

Figure 7: Injector cutaway showing manifold volume, internal passages, and instrumentation access.

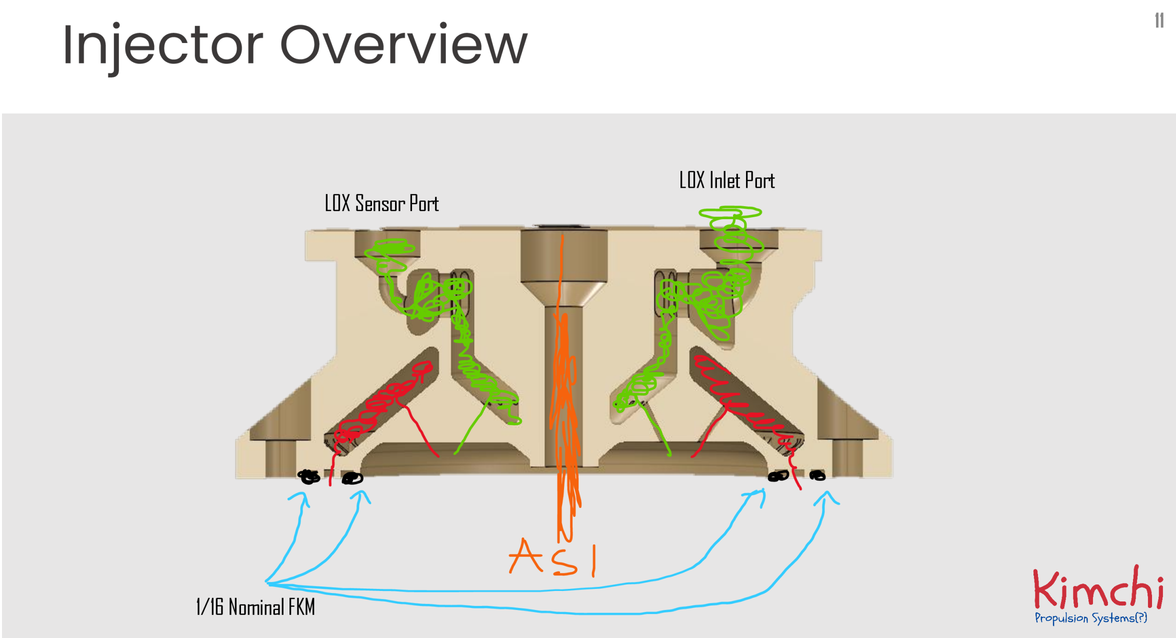

Figure 8: Annotated injector slide from the presentation deck highlighting inlet routing, sensor locations, and the internal injector geometry.

$P_{\text{inj,end}} = 6.0\,\text{bar} + 1.8\,\text{bar} = 7.8\,\text{bar}$. At full throttle, the fixed C_dA drives $P_{\text{inj,end}}$ to 26.249 bar. Equation (11) then yields $P_{\text{fuel,supply}} = 26.249\,\text{bar} + 0.498\,\text{bar} = 26.748\,\text{bar}$. Within the analysis, both propellant circuits remain below the 28 bar feed cap. Hot-fire pressure data will be compared against these predicted injector-end and supply-pressure values.

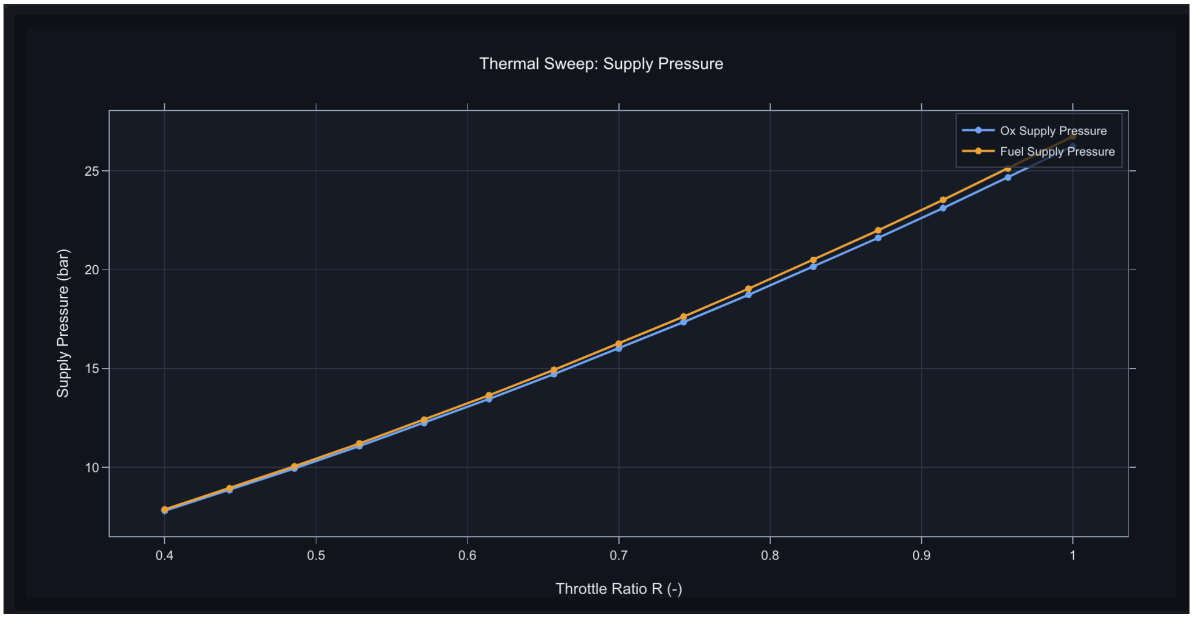

Figure 9: Required injector-end and supply pressures across the full throttle range for the fixed injector geometry.

Figures 10 and 11 reproduce the presentation-deck table and chart used to communicate how injector-end and supply pressures grow across the throttle schedule.

Throttle Per-Level Supply Pressure

20

#	Throttle	Status	Max Wall	Max Coolant	Peak Heat Flux	Ox Regen ΔP	Fuel Regen ΔP	Ox Injector-End P	Fuel Injector-End P	Ox Supply P	Fuel Supply P	Critical Zone	Issue
1	R=0.40	Completed	937.1 K	414.6 K	6.01 MW/m²	--	0.071 bar	7.800 bar	7.800 bar	7.800 bar	7.871 bar	Regenerative Zone 2	--
2	R=0.44	Completed	962.2 K	418.3 K	6.31 MW/m²	--	0.091 bar	8.849 bar	8.849 bar	8.849 bar	8.940 bar	Regenerative Zone 2	--
3	R=0.49	Completed	986.1 K	421.8 K	6.59 MW/m²	--	0.112 bar	9.940 bar	9.940 bar	9.940 bar	10.052 bar	Regenerative Zone 2	--
4	R=0.53	Completed	999.6 K	425.5 K	6.88 MW/m²	--	0.136 bar	11.072 bar	11.072 bar	11.072 bar	11.208 bar	Regenerative Zone 2	--
5	R=0.57	Completed	1003.7 K	428.5 K	7.23 MW/m²	--	0.162 bar	12.245 bar	12.245 bar	12.245 bar	12.407 bar	Regenerative Zone 2	--
6	R=0.61	Completed	1008.5 K	431.4 K	7.57 MW/m²	--	0.190 bar	13.459 bar	13.459 bar	13.459 bar	13.650 bar	Regenerative Zone 2	--
7	R=0.66	Completed	1013.8 K	434.0 K	7.91 MW/m²	--	0.220 bar	14.715 bar	14.715 bar	14.715 bar	14.935 bar	Regenerative Zone 2	--
8	R=0.70	Completed	1019.4 K	435.9 K	8.23 MW/m²	--	0.248 bar	16.012 bar	16.012 bar	16.012 bar	16.261 bar	Regenerative Zone 2	--
9	R=0.74	Completed	1025.0 K	432.6 K	8.55 MW/m²	--	0.279 bar	17.351 bar	17.351 bar	17.351 bar	17.629 bar	Regenerative Zone 2	--
10	R=0.79	Completed	1030.7 K	429.6 K	8.85 MW/m²	--	0.311 bar	18.731 bar	18.731 bar	18.731 bar	19.041 bar	Regenerative Zone 2	--
11	R=0.83	Completed	1036.4 K	427.0 K	9.15 MW/m²	--	0.345 bar	20.152 bar	20.152 bar	20.152 bar	20.497 bar	Regenerative Zone 2	--
12	R=0.87	Completed	1042.2 K	424.5 K	9.44 MW/m²	--	0.381 bar	21.614 bar	21.614 bar	21.614 bar	21.995 bar	Regenerative Zone 2	--
13	R=0.91	Completed	1047.9 K	422.2 K	9.73 MW/m²	--	0.418 bar	23.118 bar	23.118 bar	23.118 bar	23.536 bar	Regenerative Zone 2	--
14	R=0.96	Completed	1053.5 K	420.1 K	10.00 MW/m²	--	0.457 bar	24.663 bar	24.663 bar	24.663 bar	25.120 bar	Regenerative Zone 2	--
15	R=1.00	Completed	1059.2 K	418.1 K	10.28 MW/m²	--	0.498 bar	26.249 bar	26.249 bar	26.249 bar	26.748 bar	Regenerative Zone 2	--

Figure 10: Per-level supply-pressure summary from the presentation deck combining thermal outputs, injector-end pressures, and required oxidizer/fuel supply pressures.

Throttle Per-Level Supply Pressure

21

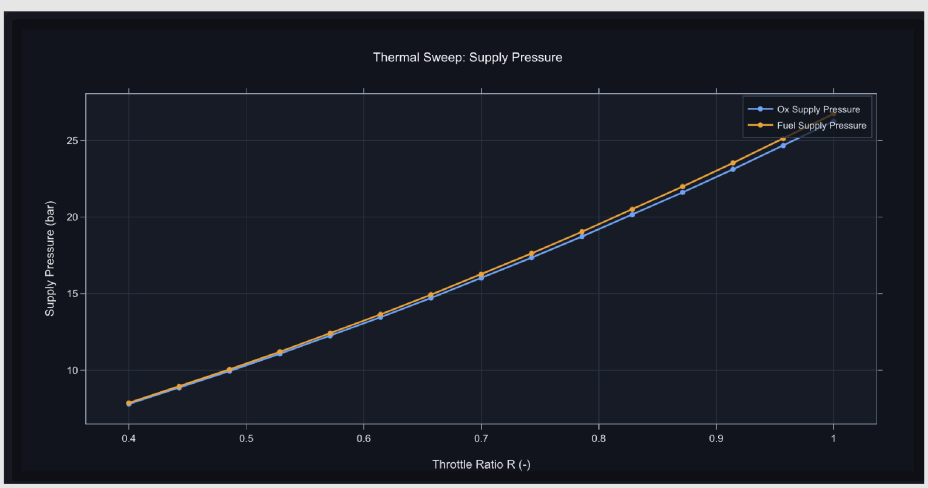

Figure 11: Per-level supply-pressure plot from the presentation deck showing the oxidizer and fuel feed requirements over the full throttle range.

3 Chamber and Nozzle Subsystem

3.1 Hot-Gas Path Geometry

3.1.1 Design Details

The combustion chamber and nozzle use a conical profile sized from the finalized thrust-plus-pressure design point. The chamber diameter is 76.36 mm, the throat diameter is 28.86 mm, the exit diameter is 40.72 mm, the chamber length is 133.6 mm, and the active hot-gas path length is 156.4 mm. The hot-wall thickness is 0.50 mm. The chamber/nozzle material is Inconel 718 through the full regenerative span.

3.1.2 Method / Model Used

The hot-gas path is generated from the finalized throat area and the conical-nozzle sizing rules,

$$A_c = 7A_t, \tag{12}$$

$$V_c = L^* A_t, \tag{13}$$

$$A_e = \epsilon A_t. \tag{14}$$

Here A_c is chamber area, V_c is characteristic chamber volume, $L^* = 1.1\,\text{m}$, and $\epsilon = 1.991$.

3.1.3 Numerical Results

Using $A_t = 6.54 \times 10^{-4}\,\text{m}^2$, Equation (12) gives $A_c = 4.58 \times 10^{-3}\,\text{m}^2$, matching the final 76.36 mm chamber diameter. Equation (14) gives $A_e = 1.30 \times 10^{-3}\,\text{m}^2$, matching the final 40.72 mm exit diameter. Table 4 and Figure 12 capture the finalized chamber and nozzle definition.

Table 4: Final chamber and nozzle geometry

Parameter	Final value
Chamber diameter	76.36 mm
Chamber area	$4.58 \times 10^{-3}\,\text{m}^2$
Throat diameter	28.86 mm
Throat area	$6.54 \times 10^{-4}\,\text{m}^2$
Exit diameter	40.72 mm
Exit area	$1.30 \times 10^{-3}\,\text{m}^2$
Expansion ratio	1.991
Chamber length	133.6 mm
Active hot-gas-path length	156.4 mm
Wall thickness	0.50 mm
Material	Inconel 718

3.1.4 Assessment

The area ratios derived from the final diameters are $A_c/A_t = 7.001$ and $A_e/A_t = 1.991$. Those values match the design inputs used in the thermochemical, thermal, and stress solutions, so the geometry definition remains analytically consistent across all modeled disciplines. As-built measurements and hot-fire data will later be compared against this geometry baseline.

Figure 12: Final hot-gas contour used for the performance, thermal, and structural closures in this CDR.

4 Regenerative Cooling Subsystem

4.1 Fuel-Cooled Chamber and Nozzle Jacket

4.1.1 Design Details

The regenerative cooling subsystem uses a single ethanol-cooled zone spanning the chamber and nozzle. Fuel enters at the exit manifold, flows upstream toward the injector, and removes heat from the full 156.4 mm active span. The cooling geometry contains 62 channels with 1.20 mm channel height, 0.80 mm minimum channel width, 3.22 mm inlet-side channel width, 0.70 mm rib thickness, 0.50 mm hot-wall thickness, and 100 µm hydraulic roughness. Figure 13 shows the cooling-jacket layout used for this thermal closure.

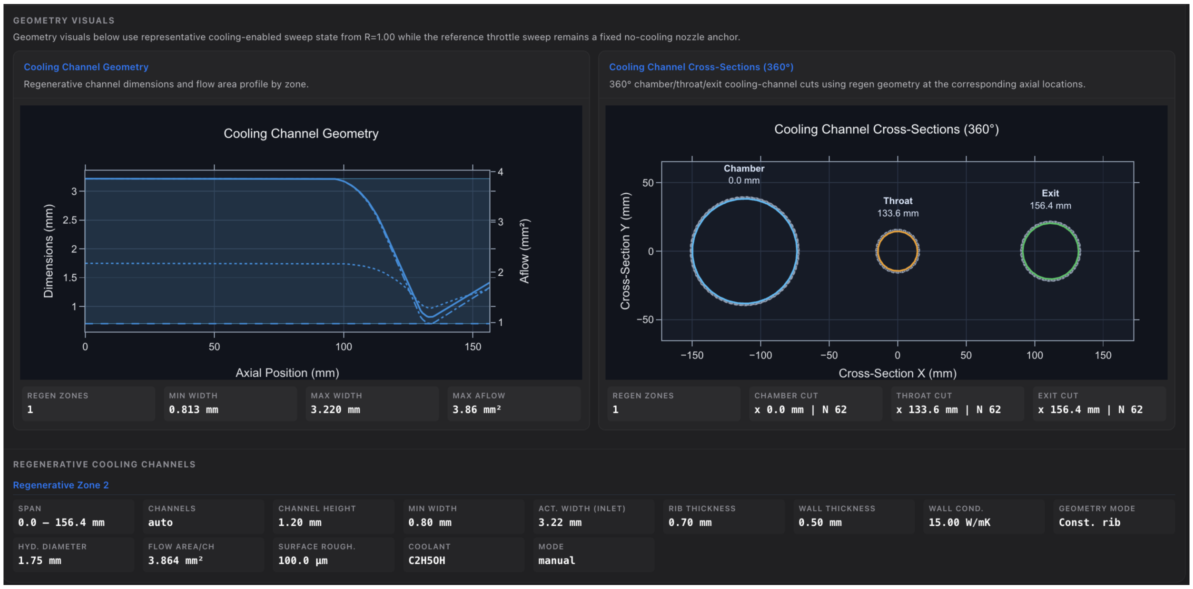

Figure 13: Released regenerative channel geometry and cross sections for the ethanol cooling circuit.

4.1.2 Method / Model Used

Gas-side loading uses Bartz convection with a 20% reduction plus radiative loading. The governing relations are

$$\sigma = \frac{1}{\left[0.5\left(\frac{T_{wg}}{T_c}\right)\left(1+\frac{\gamma-1}{2}M^2\right)+0.5\right]^{0.68}\left(1+\frac{\gamma-1}{2}M^2\right)^{0.12}}, \tag{15}$$

$$h_g = \frac{0.026}{D_t^{0.2}}\left(\frac{\mu^{0.2}C_p}{Pr^{0.6}}\right)\left(\frac{P_c}{c^*}\right)^{0.8}\left(\frac{D_t}{R_t}\right)^{0.1}\left(\frac{A_t}{A}\right)^{0.9}\sigma, \tag{16}$$

$$h_{g,\text{applied}} = 0.8\,h_g, \tag{17}$$

$$Nu = \frac{(f/8)(Re-1000)Pr}{1+12.7\sqrt{f/8}\left(Pr^{2/3}-1\right)}, \tag{18}$$

$$h_c = \frac{Nu\,k}{D_h}, \tag{19}$$

$$m = \sqrt{\frac{2h_c}{k_{wall}t_{rib}}}, \qquad \eta_f = \frac{\tanh(mL)}{mL}, \tag{20}$$

$$q'' = h_{g,\text{applied}}(T_{aw}-T_{wg}) + q''_{rad} = \eta_f h_c(T_{wo}-T_{cool}), \tag{21}$$

$$\Delta P_{\text{regen}} = \Delta P_{\text{major}} + \Delta P_{\text{minor}} + \Delta P_{\text{accel}}. \tag{22}$$

The coolant model is single-phase Gnielinski convection with Naraghi fin-efficiency correction. No boiling augmentation is applied.

Table 5: Thermal-hydraulic design inputs

Parameter	Final value
Channel count	62
Channel height	1.20 mm
Minimum channel width	0.80 mm
Inlet-side channel width	3.22 mm
Rib thickness	0.70 mm
Wall thickness	0.50 mm
Wall conductivity	15 W/(m · K)
Surface roughness	100 µm
Coolant flow direction	Exit to injector
Gas-side convection knockdown	20%

Table 6: Thermal envelope summary

Condition	Max wall temperature	Max coolant temperature	Peak heat flux	Fuel-side ΔP_{regen}	Governing region
$R = 0.40$	937.1 K	414.6 K	6.01 MW/m^2	0.071 bar	Regenerative zone 2
$R = 0.70$	1019.4 K	435.9 K	8.23 MW/m^2	0.248 bar	Regenerative zone 2
$R = 1.00$	1059.2 K	418.1 K	10.28 MW/m^2	0.498 bar	Regenerative zone 2

4.1.3 Numerical Results

4.1.4 Assessment

Tables 5 and 6, together with Figure 14, define the predicted thermal envelope. The highest wall temperature is 1059.2 K at $R = 1.00$, while the highest coolant temperature is 435.9 K at $R = 0.70$. The peak fuel-side pressure drop is 0.498 bar. Within the current model, Equation (22) closes the cooling circuit inside the feed-pressure limit used by the injector analysis, and Equation (21) remains bounded across the full throttle band. Measured injector-side temperatures and pressure data will be compared against these analytical outputs during testing.

Figures 15, 16, and 17 reproduce the per-level thermal trends from the presentation deck, making the coolant-temperature peak, regenerative pressure-loss growth, and full-throttle wall-temperature limit explicit.

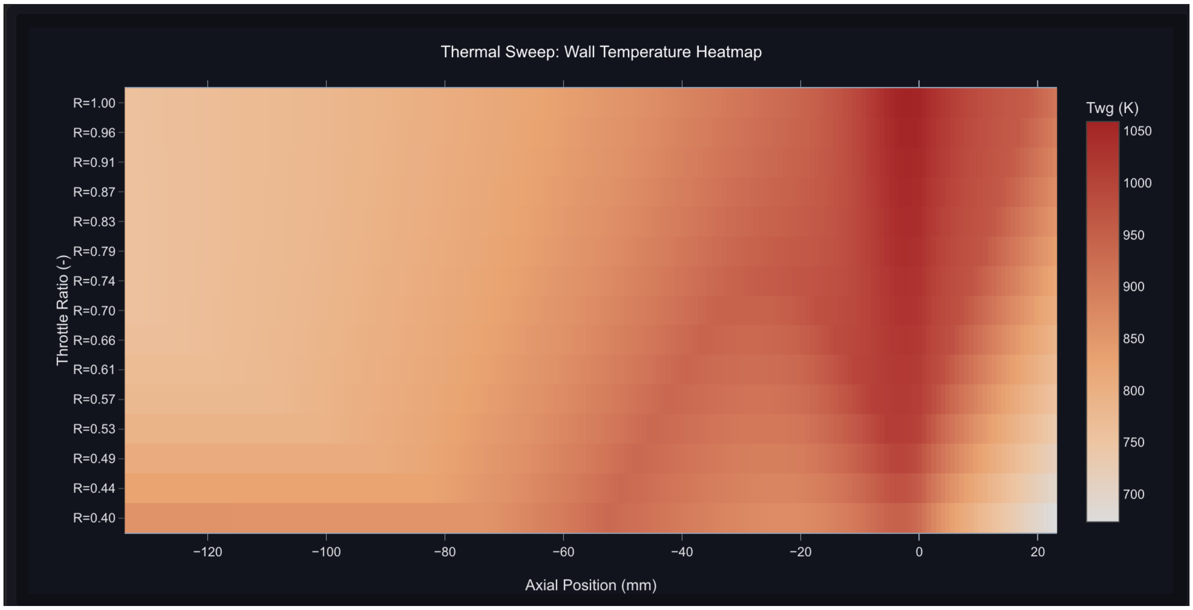

Figure 14: Wall-temperature distribution used to identify the governing regenerative region and the full-throttle thermal limit.

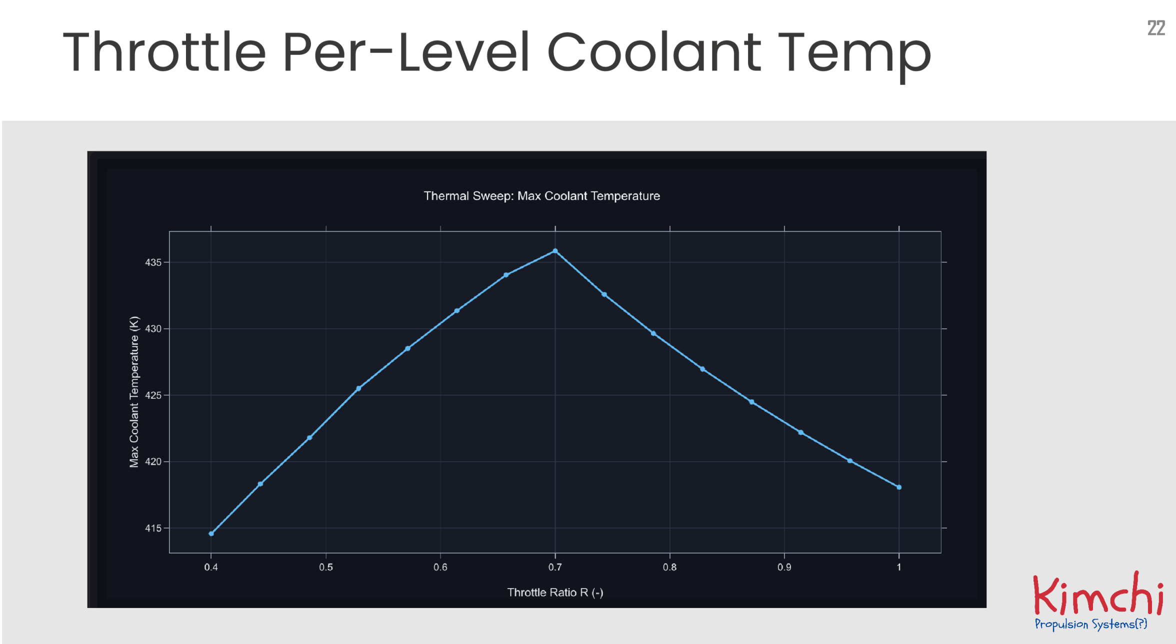

Figure 15: Per-level maximum coolant-temperature trend from the presentation deck, showing the mid-band peak identified by the regenerative thermal solution.

Throttle Per-Level Regen dP

23

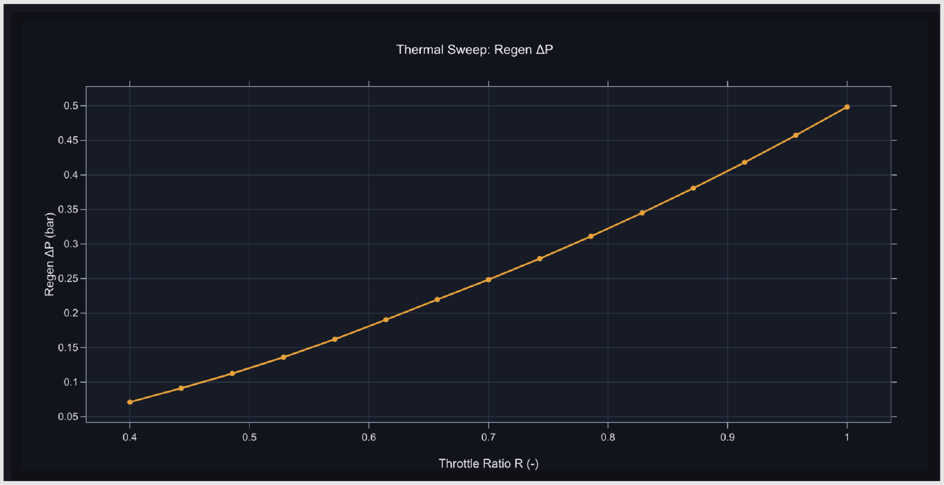

Kimchi Propulsion Systems(?)

Figure 16: Per-level regenerative pressure-drop trend from the presentation deck, showing the monotonic rise in fuel-side ΔP_{regen} with throttle.

Throttle Wall Max Twg

24

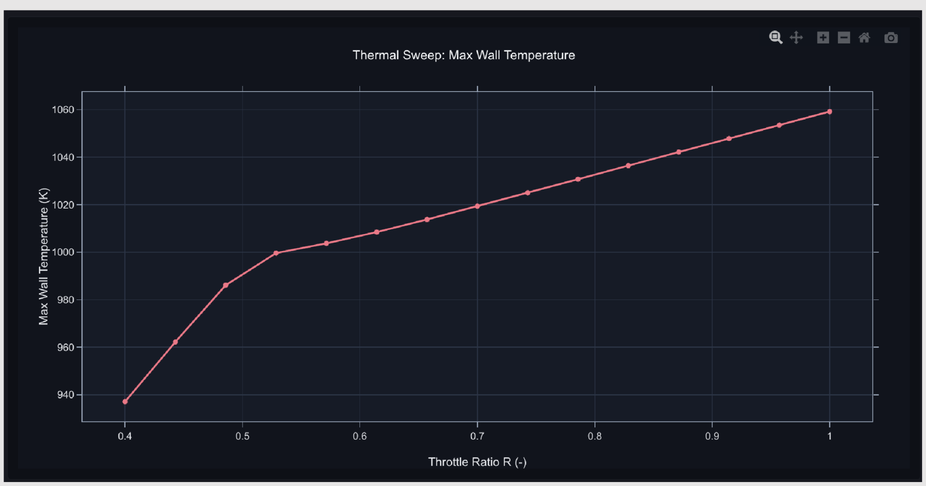

Kimchi Propulsion Systems(?)

Figure 17: Per-level maximum hot-wall temperature trend from the presentation deck, showing the governing full-throttle thermal limit.

5 Structural Integrity Subsystem

5.1 Thin-Wall Chamber Stress Closure

5.1.1 Design Details

Structural screening is carried on the thermally loaded Inconel 718 wall with direct coupling to chamber pressure and coolant-side back pressure. The governing section is the throat-side regenerative region identified by the thermal solution. The wall thickness remains 0.50 mm over the hot-gas path. Figure 18 shows the full analytical stress sweep used in this review.

5.1.2 Method / Model Used

The structural screen combines membrane pressure stress, thermal-gradient stress, and a regenerative-shell buckling check:

$$\sigma_{h,p} = \frac{\Delta P\, r}{t}, \tag{23}$$

$$\sigma_{a,p} = \frac{\Delta P\, r}{2t}, \tag{24}$$

$$\sigma_{th} = \frac{E(T)\alpha(T)\Delta T_{wall}}{2\,(1-\nu(T))}, \tag{25}$$

$$\sigma_{vm} = \sqrt{\sigma_h^2 - \sigma_h\sigma_a + \sigma_a^2}, \tag{26}$$

$$\text{FoS} = \frac{\sigma_y(T)}{\sigma_{vm,\text{governing}}}, \tag{27}$$

$$\sigma_{cr,\text{screen}} = K_d\, \frac{E(T)(t/r)}{\sqrt{3\,(1-\nu(T)^2)}}. \tag{28}$$

The buckling knockdown factor is $K_d = 0.75$. Allowables use the temperature-dependent 0.2% offset yield basis for Inconel 718.

5.1.3 Numerical Results

Table 7: Structural screening envelope

Point	Minimum FoS	Max equivalent stress	Max thermal stress	Buckling margin	Analytical screen
$R = 0.40$	2.452	351.44 MPa	342.11 MPa	7.018	Within limit
$R = 1.00$	1.412	610.23 MPa	586.86 MPa	3.901	Within limit

5.1.4 Assessment

Table 7 and Figure 18 summarize the predicted structural margins for the chamber wall. Equation (27) yields the governing full-throttle margin directly from the solved stress state: $\mathrm{FoS}_{\min} = 1.412$ at $\sigma_{vm} = 610.23\,\mathrm{MPa}$. Within this analytical screen, all 15 throttle points remain above the buckling threshold in Equation (28). The minimum buckling margin is 3.901 at the design point, so the current wall-thickness definition remains analytically admissible across the scheduled operating band. These predictions will be compared against hardware behavior and post-test inspection results before any structural acceptance claim is made.

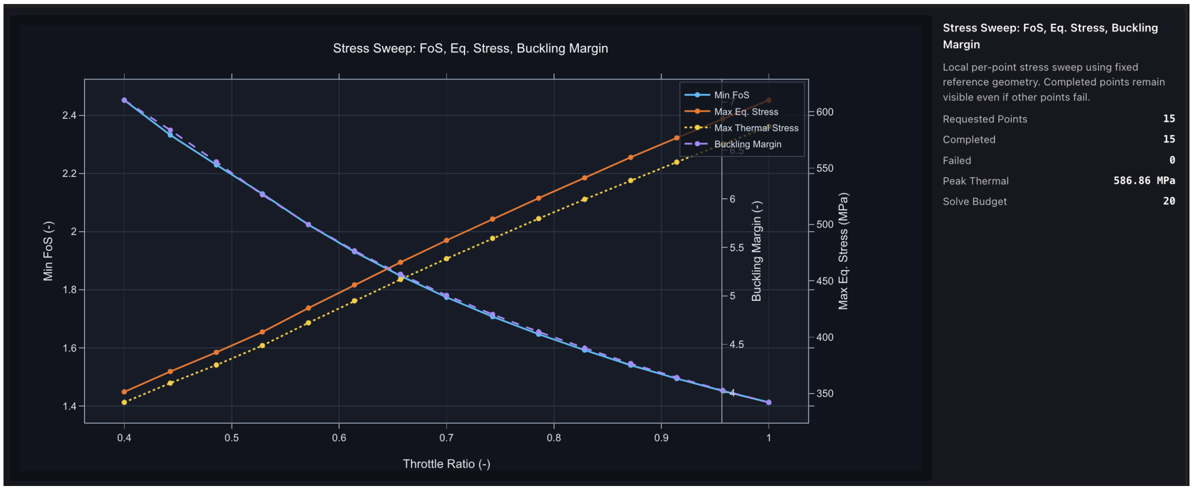

Figure 18: Equivalent stress, thermal stress, factor of safety, and buckling margin across the finalized throttle schedule.

5.2 Thrust Structure Finite-Element Screening

5.2.1 Design Details

The external thrust structure transfers engine load from the chamber/injector stack into the facility interface through a gusseted bracket and six M10 fasteners. Because this bracket geometry is not represented by the axisymmetric chamber-wall screening model, it is treated with a separate 3D finite-element screen focused on local stress concentration in the mounting features.

5.2.2 Method / Model Used

A static structural ANSYS model is used to inspect equivalent von Mises stress in the thrust bracket under the design load case. The FEA is used here as a geometry-specific screening tool for the bracket, gusset, and facility-side cutout, complementing the closed-form chamber-wall analysis summarized above. The primary outputs carried into the review are the peak stress magnitude and the location of the dominant concentration.

5.2.3 Numerical Results

Table 8: Thrust-structure FEA summary

Parameter	Reported result
Analysis type	Static structural FEA with equivalent (von Mises) stress output
Peak equivalent stress	55.6 ksi (383.0 MPa)
Highest-stress region	Facility-side cutout and adjacent mounting-hole region
Role in this CDR	Preliminary bracket screening to be compared against hardware behavior and post-test inspection

5.2.4 Assessment

Table 8 and Figure 19 summarize the current thrust-structure analysis. The plotted peak stress is 55.6 ksi (383.0 MPa), localized around the facility-side cutout and nearby mounting features, while the gusset and base plate remain lower in the displayed load case. This FEA is treated as a predictive structural screen rather than a measured hardware result. During fabrication and hot-fire operations, the bracket analysis will be compared against fastener retention, visible deformation, and post-test inspection findings before any test-correlated structural acceptance claim is made.

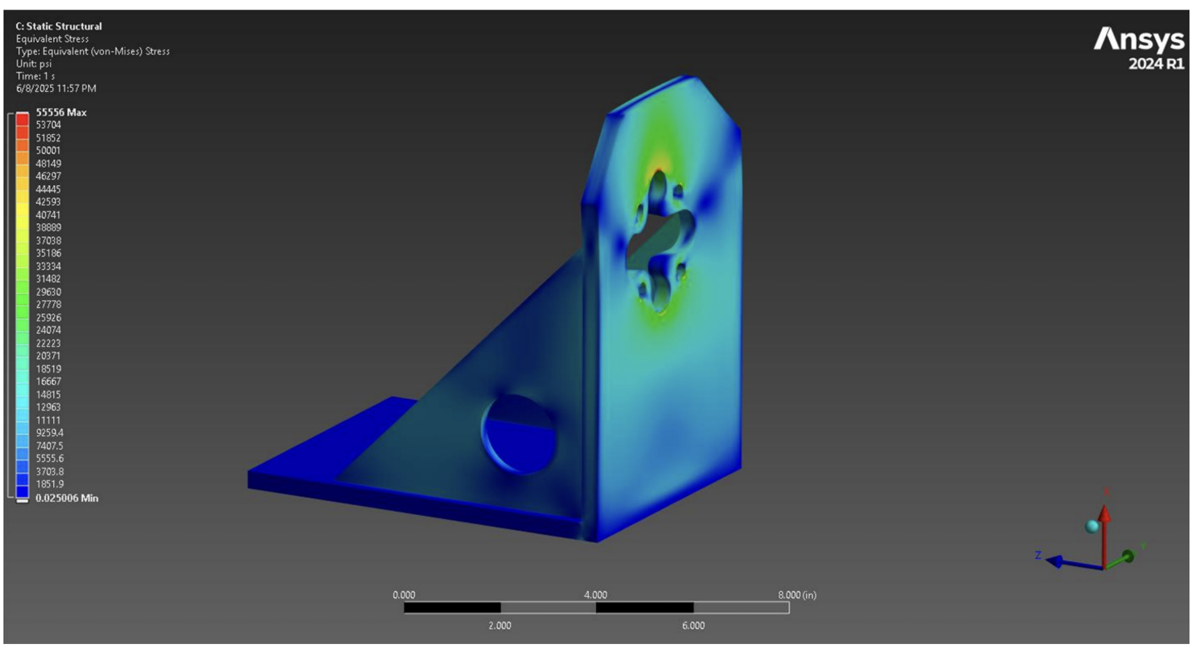

Figure 19: Static structural FEA of the thrust structure showing equivalent von Mises stress in the gusseted bracket. The displayed peak stress is 55.6 ksi (383.0 MPa), concentrated near the facility-side cutout and upper mounting region.

6 Interfaces and Integration

6.1 Mechanical, Fluid, and Facility Interfaces

6.1.1 Design Details

The engine-side mechanical stack is composed of the injector-to-chamber flange, a dedicated thrust structure, welded chamber ports, and a rear service interface that preserves access to propellant lines and instrumentation. LOX flows directly to the injector. Ethanol flows through the regenerative jacket before injector entry. The facility-side thrust-structure connection uses six M10 fasteners. Table 9 and Figures 20–23 define the integrated interface set used for this review.

6.1.2 Method / Model Used

Interface closure is assessed against three criteria: structural load path continuity, hydraulic compatibility with the pressure-fed architecture, and direct instrumentation access at the injector and chamber. Flow direction, pressure-drop allocation, and instrumentation locations are carried consistently between the analytical model and the final assembly configuration.

6.1.3 Numerical Results

Table 9: Interface definition summary

Interface	Final definition	Analytical basis
Engine to thrust structure	Dedicated thrust bracket with six M10 facility-side fasteners	Peak thrust 1300 N; local bracket screening in Figure 19
Chamber instrumentation ports	Welded pressure and temperature ports on chamber / injector assembly	Eliminates direct thin-wall port machining in the hot section
LOX feed path	Direct tank-to-injector path	Injector-end pressure equals LOX supply pressure
Fuel feed path	Exit manifold to regenerative jacket to injector	Fuel supply pressure includes Equation (22)
Igniter interface	Dedicated igniter connection at chamber head end	Supports ignition checkout and repeatable installation
Rear service access	Open access to feed lines and instrumentation leads	Leak check and turnaround servicing without hot-side disassembly

6.1.4 Assessment

The feed and structural interfaces are defined against the design-point loads and pressures predicted in Tables 3, 6, 7, and 8. Within the current analysis set, no interface requires a separate off-design configuration to support the released operating envelope. Hot-fire data, as-built inspections, and post-test hardware review will be used to compare the integrated article against these analytical interface assumptions.

Figure 22 supplements the CAD integration view with the annotated presentation slide used to communicate thrust-structure attachment and service access around the mounted engine.

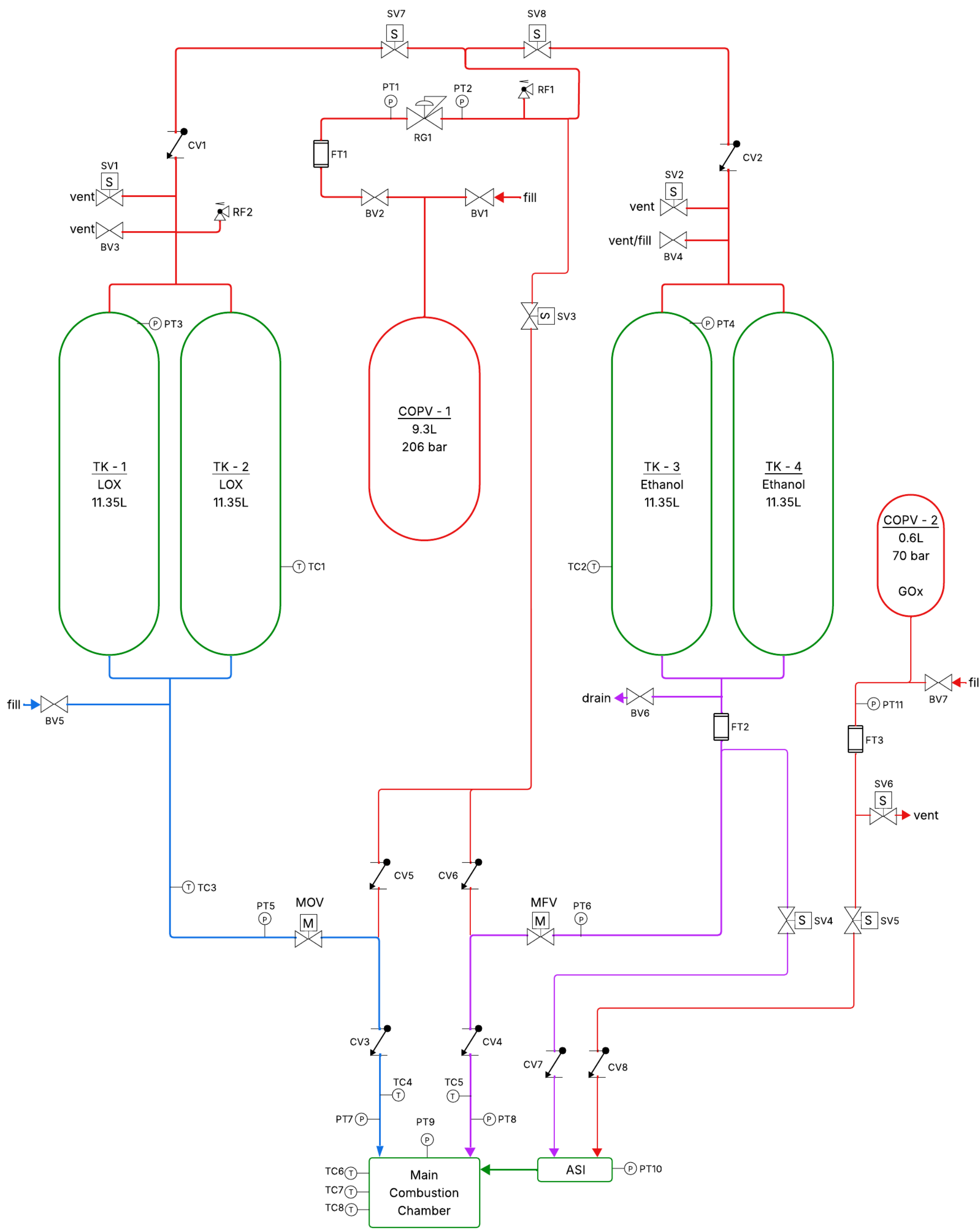

Figure 20: Propulsion-system process and instrumentation diagram aligned with the LOX direct-feed and ethanol regenerative-feed architecture used in the analysis.

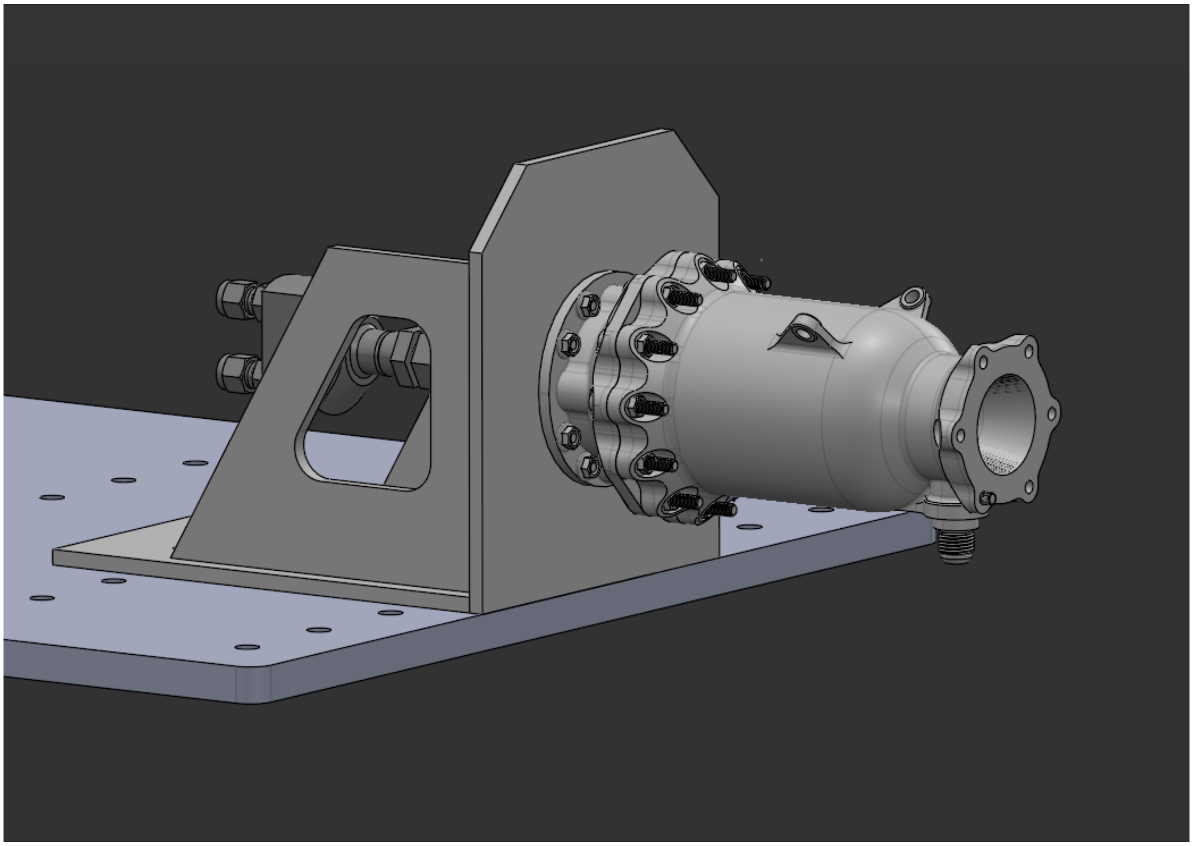

Figure 21: Engine integration with the thrust structure used for Race 2 Space facility installation.

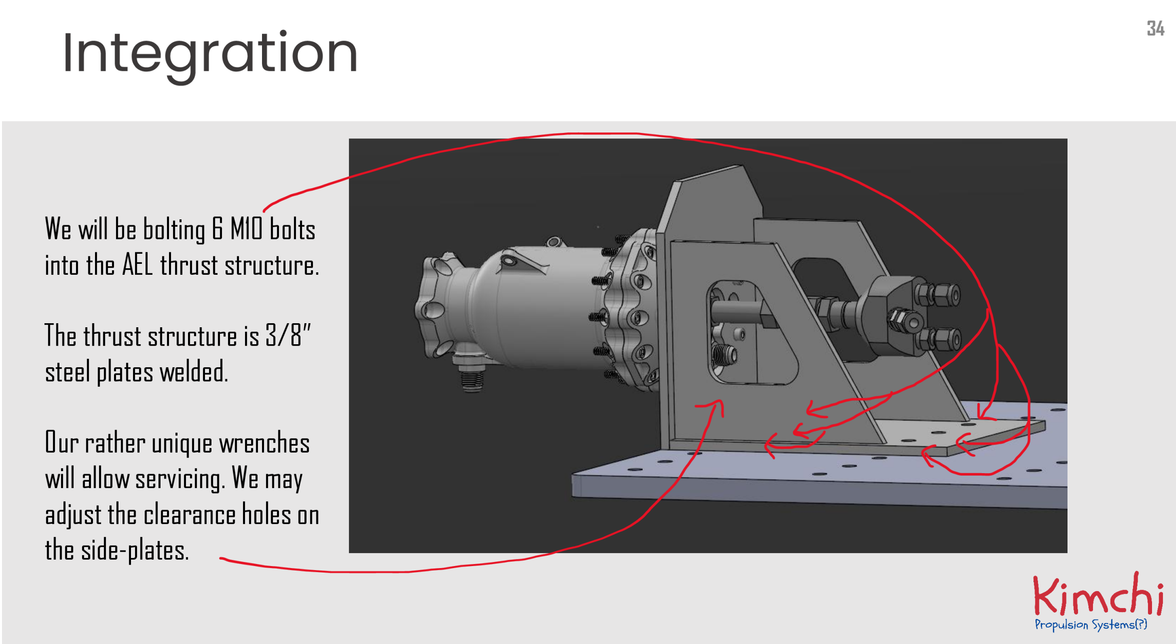

Figure 22: Annotated integration slide from the presentation deck showing the mounted engine, thrust-structure attachment, and service-access region.

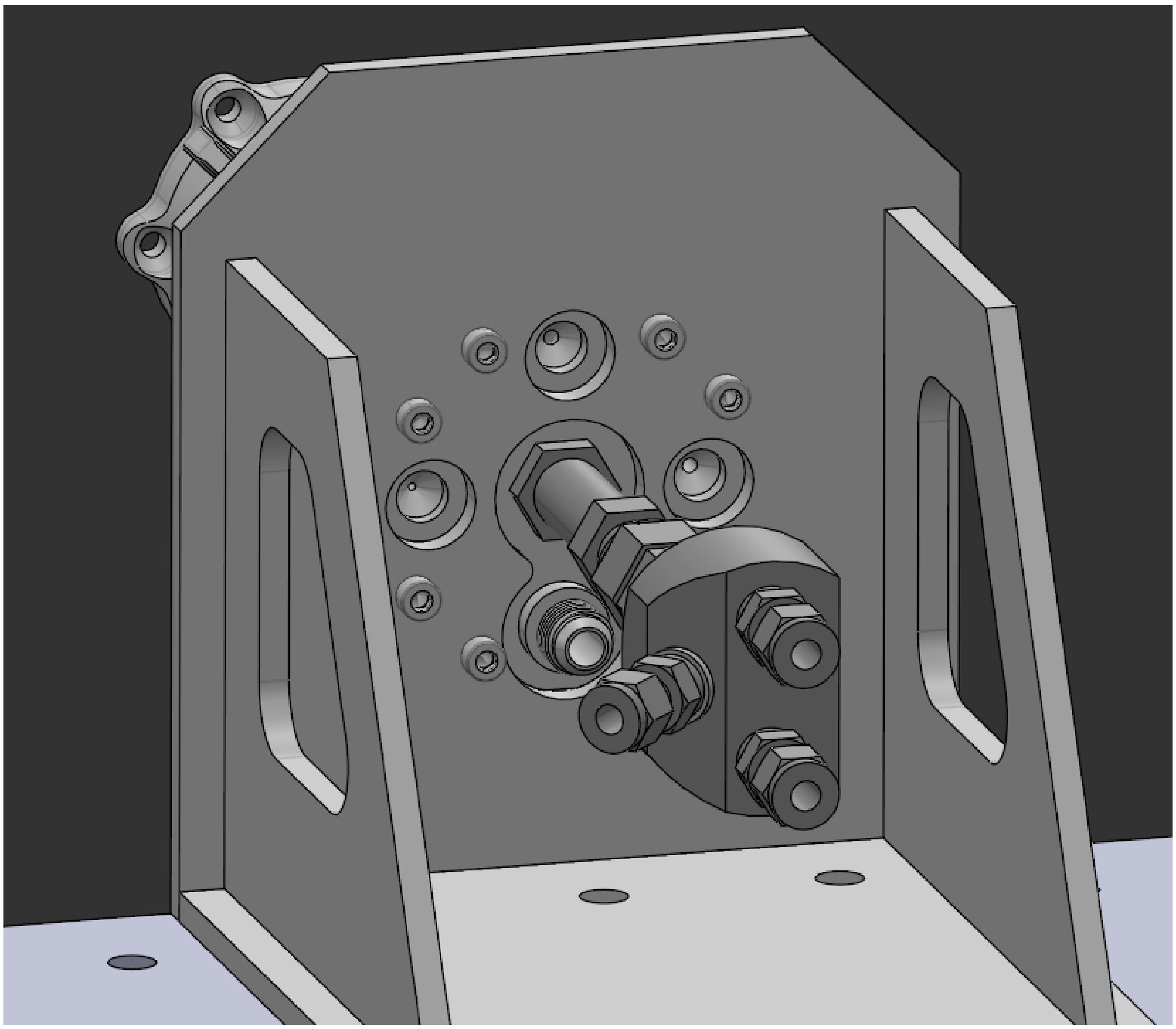

Figure 23: Rear service interface showing preserved access to feed lines, instrumentation, and the igniter connection.

7 Instrumentation and Data Acquisition

7.1 Hot-Fire Measurement Set

7.1.1 Design Details

The released instrumentation set is restricted to channels required for planned test-to-analysis comparison, safety monitoring, and performance characterization. The measurement set covers chamber pressure, injector-side propellant pressures, and injector-side propellant temperatures. Table 10 defines the released sensor set.

7.1.2 Method / Model Used

Instrumentation is mapped to the dominant analytical uncertainties: chamber-pressure closure, injector pressure-drop closure, and fuel/oxidizer thermal boundary conditions at the injector. Sensor placement is therefore concentrated at the chamber head end and the injector feed interfaces.

Figure 24 shows the annotated chamber-head-end port view from the presentation deck, making the pressure, temperature, and feed interfaces easier to identify.

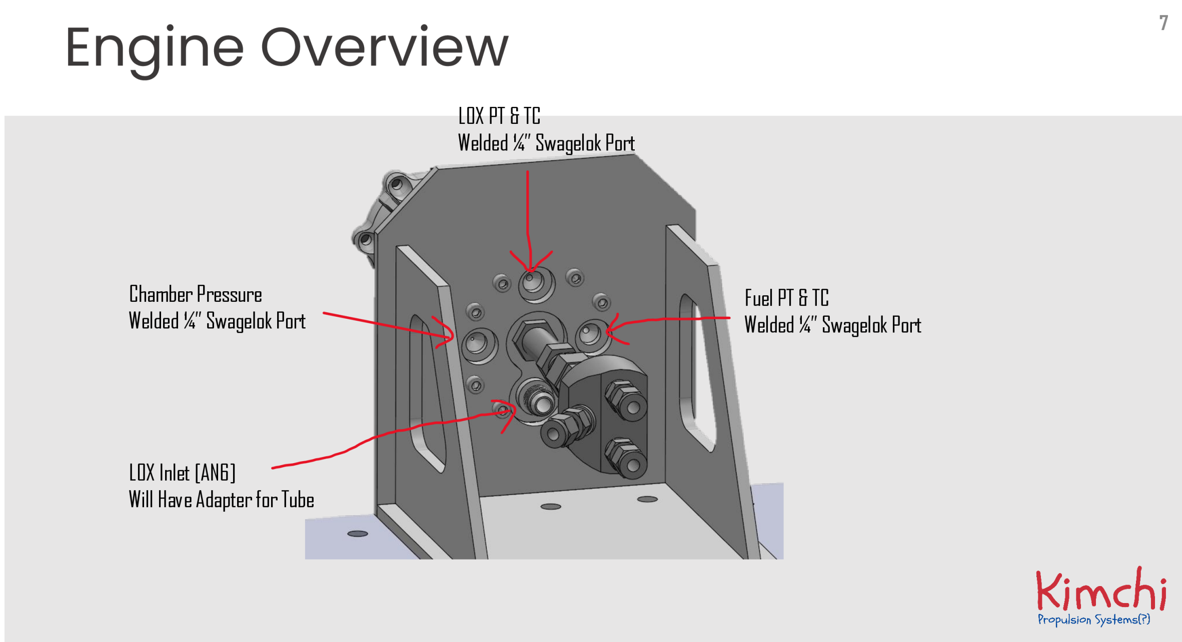

Figure 24: Annotated chamber-head-end slide from the presentation deck showing the chamber-pressure port, propellant pressure/temperature ports, and LOX inlet interface.

Table 10: Released instrumentation and purpose

Measurement	Sensor specification	Quantity	Planned data use
Chamber pressure	4–20 mA pressure transmitter, 0–40 bar, 24 VDC	1	Chamber-pressure history, ignition transient review, and thrust-model closure
Fuel injector pressure	4–20 mA pressure transmitter, 0–40 bar, 24 VDC	1	Fuel-side injector drop and regenerative pressure-loss closure
LOX injector pressure	4–20 mA pressure transmitter, 0–40 bar, 24 VDC	1	Oxidizer-side injector drop and feed-balance tracking
Fuel injector temperature	Type K thermocouple with miniature connector	1	Fuel-side thermal boundary condition near the injector
LOX injector temperature	Type E thermocouple with miniature connector	1	Cryogenic-side thermal boundary condition near the injector

7.1.3 Numerical Results

7.1.4 Assessment

The five-channel instrumentation set in Table 10 provides the minimum measurements needed to compare chamber-pressure tracking, injector hydraulic losses, and injector-side thermal boundary conditions against the regenerative model. No measurement in the released set is redundant with the planned hot-fire comparison objectives.

8 Test Plan

8.1 Qualification-by-Test Sequence

8.1.1 Design Details

The test campaign progresses from ignition confirmation to design-point static fire and then to a composite throttle schedule. Each test is executable with the finalized hardware configuration and the released instrumentation set. Table 11 lists the full campaign definition.

8.1.2 Method / Model Used

The test sequence is structured to compare ignition behavior, design-point performance, and throttling response against the analytical predictions in that order. Each test objective is mapped to a subsystem-level data-comparison target so the campaign can retire risk without redesign between test points.

Table 11: CDR hot-fire test matrix

Test	Condition	Duration	Instrumentation required	Acceptance metric	Primary comparison focus
Test A: ignition check	$R = 0.40$, 440.6 N, 6.0 bar, LOX supply 7.80 bar, fuel supply 7.871 bar	2 s	Full released set	Stable ignition, valid chamber-pressure trace, no abnormal injector pressure excursion	Injector, ignition, DAQ
Test B: design-point static fire	$R = 1.00$, 1300.0 N, 15.0 bar, LOX supply 26.249 bar, fuel supply 26.748 bar	2 s design-point hold	Full released set	Stable chamber pressure, bounded thermal response, no structural exceedance indicators	Full engine system
Test C: composite throttle sweep	40 % to 100 % throttle schedule with ramps and repeated holds	20 s total	Full released set	Chamber-pressure tracking across the schedule and no feed-system saturation	Throttle control, thermal-hydraulic closure

8.1.3 Numerical Results

8.1.4 Assessment

Test A will compare ignition behavior and sensor health against the startup expectations derived from the low-throttle operating point. Test B will compare design-point chamber pressure, feed pressure, and thermal response against the full-throttle predictions. Test C will compare the fixed-geometry throttle schedule, injector hydraulic closure, and regenerative pressure-loss model across the full operating band. The campaign therefore provides the first direct opportunity to compare the present analysis set against hardware data without changing the geometry between tests.

9 Readiness Assessment

9.1 Residual Risk and Release Status

9.1.1 Design Details

The design is defined as a fixed hardware configuration with closed geometry, closed feed-pressure limits, closed regenerative cooling, closed structural screening, and an executable hot-fire sequence. Remaining risk is concentrated in fabrication and test execution rather than in unresolved configuration decisions.

9.1.2 Method / Model Used

Readiness is assessed against four analysis-based release criteria: final geometry definition, subsystem integration consistency, positive margin on safety-critical hardware, and an executable test matrix tied to planned data-comparison objectives.

9.1.3 Numerical Results

The current analysis set indicates that the design meets the numerical gates consolidated from Tables 1, 3, 6, 7, and 8:

- design thrust of 1300.0 N at 15.0 bar chamber pressure,
- continuous throttle envelope from 440.6 N to 1300.0 N,
- peak regenerative pressure loss of 0.498 bar,
- peak wall temperature of 1059.2 K,
- minimum structural factor of safety of 1.412,
- minimum buckling margin of 3.901,
- maximum fuel supply pressure of 26.748 bar against a 28.0 bar cap.

9.1.4 Assessment

On the basis of the current analytical work, the Kimchi engine is judged ready to proceed to fabrication, assembly, checkout, and hot-fire testing as defined. Remaining execution risks are weld quality, assembled leak tightness, igniter checkout, transient behavior during first-fire operations, and correlation of the analytical predictions with measured data. Those risks are reduced by the defined inspection and test sequence rather than by further geometry changes, and the final acceptability of the design remains subject to comparison with as-built hardware and hot-fire results.